Earth and Planetary Science Letters 622 (2023) 118403

Contents lists available at ScienceDirect

Earth and Planetary Science Letters

journal homepage: www.elsevier.com/locate/epsl

Boron geochemistry reveals the evolution of Dead Sea brines

Hana Jurikova [a,b,*], Simon J. Ring [c], Michael J. Henehan [c,d], Ina Neugebauer [a], Birgit Schröder [a], Daniela Müller [a], Markus J. Schwab [a], Rik Tjallingii [a], Achim Brauer [a,e], Cécile Blanchet [a]

[a] GFZ German Research Centre for Geosciences – Helmholtz Centre Potsdam, Section Climate Dynamics and Landscape Evolution, Telegrafenberg, 14473, Potsdam, Germany
[b] University of St Andrews, School of Earth and Environmental Sciences, Bute Building, Queen's Terrace, St Andrews, KY16 9TS, United Kingdom
[c] GFZ German Research Centre for Geosciences – Helmholtz Centre Potsdam, Section Earth Surface Geochemistry, Telegrafenberg, 14473, Potsdam, Germany
[d] University of Bristol, School of Earth Sciences, Wills Memorial Building, Queen's Road Bristol, BS8 1RJ, United Kingdom
[e] University of Potsdam, Institute of Geosciences, Karl-Liebknecht-Str. 24–25, 14476, Potsdam, Germany

ARTICLE INFO

Article history:
Received 3 July 2023
Received in revised form 7 September 2023
Accepted 11 September 2023
Available online xxxx
Editor: A. Jacobson

Keywords:
boron cycle
boron isotope budget
seawater evolution
Pliocene Sedom Lagoon
Pleistocene Lake Lisan
lacustrine authigenic aragonites

ABSTRACT

Well-known for their geological and natural singularity, the Dead Sea brines evolved from a marine ingression of the Mediterranean during the Pliocene. Dead Sea brines are currently almost ten times more concentrated than seawater and have a unique chemical composition with high boron isotope values ($\delta^{11}B_{brine}$ = ~57‰). However, little is known on how these values were attained and their underlaying driving processes. Here we use boron isotopes ($\delta^{11}B$) combined with B/Ca and B/Li of lacustrine authigenic aragonites from the deep basin drill-core ICDP 5017-1, and Ein Gedi and Masada profiles to reconstruct past brine conditions. Comparing reconstructed $\delta^{11}B_{brine}$ from two key periods of contrasting hydro-climatic regimes we find that the brines of the late Holocene Dead Sea were enriched in ^{11}B ($\delta^{11}B_{brine}$ = ~60‰) relative to its glacial precursor Lake Lisan (~57‰). With the aid of boron cycle modelling, we quantify the main boron fluxes in the basin. We show that the post-glacial $\delta^{11}B_{brine}$ enrichment is best explained by overall reduction of freshwater inflow to the lake and coeval increase in ^{10}B sink through boron co-precipitation in evaporitic deposits and boron loss in atmospheric water vapour, consistent with the onset of warmer and drier climate in the Eastern Mediterranean during the Holocene. On geological time scales, adsorption of ^{10}B on clastic sediments has acted as an important ^{10}B sink and can explain the evolution of the high $\delta^{11}B_{brine}$ values.

1. Introduction

Due to the large mass difference between its two stable isotopes (^{10}B and ^{11}B) and its high geochemical reactivity, boron (B) is significantly fractionated in nature, making it an invaluable tracer of Earth processes ranging from subduction to weathering. In lacustrine systems, the pronounced difference between the B isotopic composition of brines ($\delta^{11}B_{brine}$) derived from seawater ($\delta^{11}B_{seawater}$ = 39.6‰; Lemarchand et al., 2000; Foster et al., 2010) and those bearing signatures of continental crust ($\delta^{11}B_{crust}$ values range between −20 to 10‰; Trumbull and Slack, 2017) has meant boron isotope ratios were traditionally considered as a tracer to distinguish marine vs. non-marine origin of evaporitic environments (Swihart et al., 1986; Vengosh et al., 1992). There are numerous examples of this difference being leveraged to characterise brine systems worldwide. For instance, the salt lakes of the Qaidam Basin in China record a relatively low $\delta^{11}B_{brine}$ (−0.7 to 10.9‰) diagnostic of a non-marine origin primarily influenced by nearby granitic rocks (Vengosh et al., 1995). By contrast, salt lakes across South and Western Australia with comparatively high $\delta^{11}B_{brine}$ (between 27.6−48.7‰) have been interpreted as being dominated by cyclic salt input derived from seawater, modified by the precipitation and dissolution of halites and other evaporitic minerals (Vengosh et al., 1991a). Enriched yet variable $\delta^{11}B_{brine}$ values in Antarctica (ranging from 12.3 to 51.4‰) are interpreted as reflecting a mixture between a marine-like source and glacier meltwater (Leslie et al., 2014). The $\delta^{11}B_{brine}$ of lacustrine systems thus reflects water origin, over which fingerprints from hydro-geochemical processes are superimposed.

The hypersaline lacustrine body filling the Dead Sea basin began with an ingression of the Mediterranean into the Jordan Rift

* Corresponding author at: University of St Andrews, School of Earth and Environmental Sciences, Bute Building, Queen's Terrace, St Andrews, KY16 9TS, United Kingdom.
E-mail address: hj43@st-andrews.ac.uk (H. Jurikova).

https://doi.org/10.1016/j.epsl.2023.118403

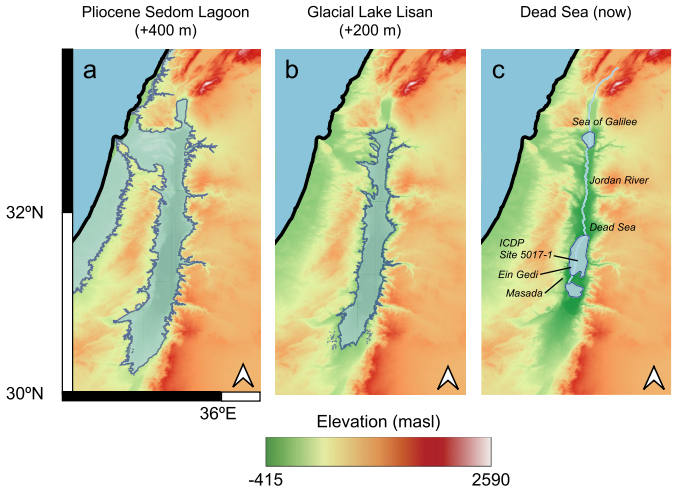

Fig. 1. Topographic map of the Dead Sea basin in the Levant region showing the elevation (masl) and the lake during its stages as; a) Pliocene Sedom Lagoon, b) glacial Lake Lisan, and c) modern Dead Sea with sampling locations indicated.

Valley during the Pliocene forming the Sedom Lagoon. The Dead Sea brines are a residual product of the evaporated seawater that precipitated evaporitic minerals and interacted with sediments and the bedrock of Cenomanian and Turonian limestones, and later also the Mount Sedom salt diapir (Zak, 1967; Katz and Starinsky, 2009; Levy et al., 2019). Although of marine origin, the $\delta^{11}B_{brine}$ of the modern Dead Sea (between 55.7−57.4‰) and associated hot springs (55.2−55.7‰) is strongly enriched relative to seawater (39.6‰), making it one of the most ^{11}B-enriched natural reservoirs known (Vengosh et al., 1991b). Based on the high $\delta^{11}B_{brine}$ values, but low B/Li ratios (∼2−3 mol/mol in comparison to ∼17 mol/mol in seawater), used as an indicator of changes in B content as Li behaviour is thought to be more conservative, Dead Sea brines have been considered to have derived from seawater through evaporation, precipitation of salts and interaction with clay minerals (Vengosh et al., 1991b). Understanding past boron budgets of the lake would allow us to trace its evolution through time and its underlaying driving processes. However, thus far and to the best of our knowledge, no attempts have been made to infer past $\delta^{11}B_{brine}$; indeed, even past $\delta^{11}B_{seawater}$ remains poorly constrained due to challenges associated with the reconstruction of this parameter.

The well-preserved geologic record of the Holocene Dead Sea and its glacial precursor Lake Lisan (14 ka to 70 ka BP; Kaufman, 1971) is characterised by annual laminations – varves – composed of alternating layers of authigenic aragonite and detritus (Neugebauer et al., 2014; Ben Dor et al., 2019). Aragonite appears as thin laminae, usually of several hundred µm to 1 mm thick, preserved in its primary state thanks to the dry climate and high Mg/Ca of interstitial soluble salts (Stein et al., 1997). Thought to occur annually in the past, aragonite precipitation under modern conditions is rare due to increasing water stress from anthropogenic water consumption leading to a hypersaline state. The last so-called 'whiting event' during which aragonite formed in the Dead Sea was reported in 1959 (Neev and Emery, 1967), hampering a direct study of aragonite formation today. The rich aragonite sequences of Dead Sea geologic record, however, leave behind a promising archive of brine conditions during the major transition in water balance and regional hydro-climatic conditions that accompanied the shift from lake level high-stand during the Last Glacial Maximum (LGM) to a low-stand at the onset of the Holocene (Torfstein et al., 2013; Kiro et al., 2017; Fig. 1).

We present $\delta^{11}B$ (alongside Element/Ca, $\delta^{13}C$ and $\delta^{18}O$) from authigenic aragonite from the sedimentary record of the Dead Sea basin during the two key periods of contrasting hydroclimatic regimes – the late glacial and the late Holocene. We show that the lacustrine aragonites offer a unique opportunity for reconstructing past $\delta^{11}B_{brine}$ and with the aid of mass balance modelling unravel the main process driving the boron cycle in the basin and the evolution of the brines.

2. Materials and methods

2.1. Samples and geochemical analyses

Authigenic aragonite was hand-picked from single varve aragonite laminae of sediment cores and outcrop profiles recovered from three different sites within the Dead Sea basin (Fig. 1). Late Holocene (∼1–4 ka BP) samples were collected from the core recovered during the Dead Sea Deep Drilling Project (DSDDP) within the ICDP program framework in the deep northern basin at site 5017-1 in 2010 (Neugebauer et al., 2014), and the shallow profile 'DSEn' from the western margin of the lake at Ein Gedi (Migowski et al., 2006; Neugebauer et al., 2015). For further details on the cores the reader is referred to the aforementioned publications, which include a detailed description of the lithostratigraphy, microfacies and X-ray fluorescence spectroscopy (XRF). The depths at which samples were collected are provided in the Supplement. The age model for the ICDP core 5017-1 and Ein Gedi was constructed using previously published radiocarbon ages (Neugebauer et al., 2014, 2015; Kitagawa et al., 2017) and modelled with the OxCal Program (Ramsey, 2008). In addition, several samples spanning the late glacial interval were measured from a new profile from the southwestern Masada formation, recovered during a campaign to the Dead Sea in 2018 (Müller et al., 2022). Altogether, a composite profile of about 300 cm long was retrieved at Masada, starting 23 cm below the top of the Additional Gypsum Unit (AGU; Torfstein et al., 2008). The samples used in this study were taken at 5 to 10 cm intervals between 82 and 427 cm of the profile (below the top of the AGU) sampled at 5 to 10 cm intervals, with the exception of a hiatus between 160 and 380 cm formed by the Upper Gypsum Unit (UGU, Torfstein et al., 2008). A revised age model based on tephrochronology, varve counting and radiocarbon ages dates this sediment section between approximately 13 to 17 ka BP (Müller et al., 2022; Neugebauer et al., 2021).

Sample preparation and geochemical analyses were carried out at the GFZ German Research Centre for Geosciences – Helmholtz Centre Potsdam, in Potsdam, Germany. Approximately 10 mg of $CaCO_3$ powder was carefully hand-picked from single varve aragonite laminae using a scalpel and inspected under a light microscope for microfacies composition. In most instances, the sampled material contained pure authigenic aragonite only. Few samples containing an admixture of detrital carbonate or gypsum were also found and analysed for comparison (see Supplement). In total 57 aragonite, 50 detrital and 13 mixed samples from the ICDP Deep core, Ein Gedi profile, and from Masada profile were measured for their stable carbon ($\delta^{13}C$) and oxygen isotope ($\delta^{18}O$) composition. Out of these, 19 aragonite and 2 detrital samples from the ICDP core 5017-1, 9 aragonite samples from Ein Gedi, and 10 samples from Masada were selected for elemental and boron isotope ($\delta^{11}B$) measurements. Selected specimens were further imaged at a high-resolution using a ZEISS Ultra Plus Scanning Electron Microscope (SEM) employing In-lens and SE-Detector for high-resolution and an Annular Backscatter Detector (AsB) for material contrast. SEM imaging of selected aragonite samples revealed exquisite preservation and purity of aragonite at all sites – ICDP core 5017-1, Ein Gedi and Masada (Fig. 2).

For $\delta^{13}C$ and $\delta^{18}O$ analyses an aliquot of ∼0.5 mg of $CaCO_3$ was weighed into a glass tube, rinsed three times with ultrapure water (Milli-Q, 18.2 MΩ) to remove salts, and subsequently dried at 60 °C. Measurements were performed after a digestion

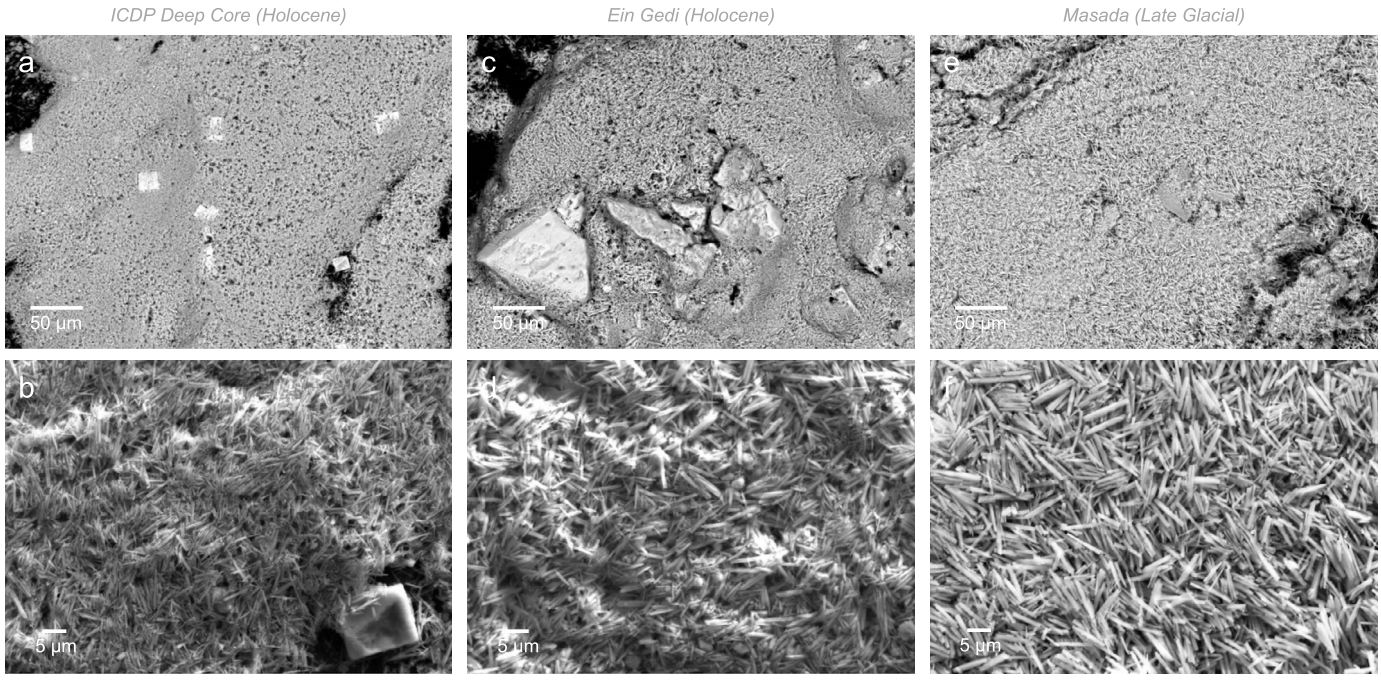

Fig. 2. Aragonite laminae viewed under scanning electron microscope (SEM). In top panels are backscatter overviews and in bottom panels secondary electron close-ups on the same samples; a–b) ICDP core 5017-1; c–d) Ein Gedi; and e–f) Masada. Note the pristine aragonite needles among salt crystals.

with 103% H_3PO_4 at 70 °C, either using a DELTA^{plus} XL isotope ratio mass spectrometer (IRMS) coupled to a Gasbench II (Thermo Fisher Scientific) or a MAT253 IRMS with an automated carbonate preparation device KIEL IV (Thermo Fisher Scientific). Both $\delta^{13}C$ and $\delta^{18}O$ carbonate values are expressed in delta notation relative to VPDB in per mille. The analytical precision (1σ) evaluated by repeated measurements of international (NBS19, IAEA-CO-1) and internal (C1) carbonate standards was better than 0.08‰ for $\delta^{13}C$ and $\delta^{18}O$.

An aliquot of ~2 mg $CaCO_3$ was collected into pre-cleaned 1.5 ml centrifuge tubes for determination of Element/Ca and $\delta^{11}B$. Powders were first repeatedly rinsed with Milli-Q, and subsequently treated with a reductive and oxidative cleaning step in an ultrasonic bath at 80 °C. To remove any potential ferromanganese oxide coatings, a reductive solution of hydroxylamine hydrochloride buffered with 0.1 M NH_4OH was applied (500 µl per sample). Organic matter was oxidised with 1% H_2O_2 buffered with 0.1 M NH_4OH (500 µl per sample). Cleaned samples were transferred into 1.5 ml centrifuge PFA (Teflon) vials and treated with a weak acid leach (0.5 mM HNO_3, 250 µl per sample) for 30 seconds to remove any re-adsorbed contaminants. Finally, we dissolved the samples in 0.5 M HNO_3 with the aid of ultrasonication using about 100–200 µl of 0.5 M HNO_3 to achieve complete dissolution. An aliquot of 10% of each dissolved sample was analysed for major and trace elements (Li, B, Na, Mg, Al, Ca, Mn, Sr, Cd, Ba, Nd, U) on an Element 2 ICP-MS (Thermo Scientific). The reproducibility (2RSD) on the relevant ratios was better than 4% determined by repeated measurement of in-house consistency standards.

Prior to boron isotope analyses, boron was purified from sample carbonate matrix on micro-columns (20 µl resin volume) using boron specific anion exchange resin Amberlite IRA 743 crushed and sieved to 63–106 µm. Given the pH dependent boron retention on the resin, samples were buffered to a pH of 5 using 1 M ammonium acetate–~1.2 M acetic acid buffer (using a buffer volume twice that of 0.5 M HNO_3 in which the sample was dissolved) and carefully loaded onto the columns. Carbonate matrix and buffer were eluted during repeated rinses with Milli-Q, before purified boron was collected with 0.5 M HNO_3 (600 µl in total; yielding >98% boron recovery). To ensure that no significant amount of sample remained on the column after the collection, boron content of elution tails was determined (representing <2% of the total boron in the sample; for most samples the tails were <1% and few of the tails closer to 2% also included standards corroborating that the higher tail values did not affect their $\delta^{11}B$). For each column batch, the boron content of a total procedural blank (TPB) was determined (with average TPB amounting ~71 ± 46 pg; <1% of the sample size) and one or two carbonate standards were processed along with samples. Purified boron samples were stored in PFA vials sealed with Parafilm, and prior to analysis (typically within few days of the column procedure) were diluted to 20 ppb and spiked with ultrapure HF to 0.3 M to aid B washout.

Boron isotopic composition was determined on a Neptune Plus MC-ICP-MS (Thermo Scientific) in the Helmholtz Laboratory for the Geochemistry of the Earth Surface (HELGES) at the GFZ Potsdam. Our setup combined an ESI PFA 75 µl min^{-1} nebuliser connected to a PFA double pass barrel spray chamber, and an ASX-110FR Flowing Rinse Micro Autosampler (Teledyne CETAC). To overcome the notorious washout problems associated with B measurements on ICP-MS, we used 0.5M HNO_3–0.3M HF wash solution (following Misra et al., 2014; Zeebe and Rae, 2020), which effectively reduced B memory to background values (<2 mV) within ~1 minute of wash time. Instrumental mass bias was corrected by standard-sample bracketing with a 20 ppb standard NIST SRM 951 boric acid that consequently converts $^{11}B/^{10}B$ ratios to delta notations. Each analysis consisted of 60 cycles of 2 s integration time, simultaneously collecting masses 11 and 10 in Faraday cups H3 and L3, respectively, both equipped with 10^{13} Ω resistors. The typical signal intensity after optimisation for mass bias stability ranged from 10–20 mV per ppb B on mass 11.

External reproducibility (2σ) on $\delta^{11}B$ measurements was better than 0.36‰, as assessed by repeated measurements of purified carbonate reference materials processed through columns with each batch of samples, and at similar [B] to the samples (10–20 ng). For the international coral standard JCp-1 $\delta^{11}B = 24.41 \pm 0.36$ (n = 3), for JCt-1 $\delta^{11}B = 16.12 \pm 0.13$ (n = 2), and our in-house brachiopod standard MVS-1 $\delta^{11}B = 15.94 \pm 0.32$ (n = 3), in good

agreement with other laboratories (Jurikova et al., 2019; Gutjahr et al., 2020; Wang et al., 2010; Buisson et al., 2021). The average $\delta^{11}B$ of TPBs was ~0‰.

2.2. Reconstruction of $\delta^{11}B_{brine}$ from lacustrine aragonites

Late glacial (~13–15 ka BP) and late Holocene (1–4 ka BP) $\delta^{11}B_{brine}$ values were reconstructed from $\delta^{11}B$ measurements of authigenic aragonites ($\delta^{11}B_{arag}$). Provided that a brine's pH and pK_B^* at time of aragonite precipitation is known or can be constrained, as shown subsequently, and that aragonite reflects the $\delta^{11}B$ of ambient borate ion faithfully (as shown by Noireaux et al., 2015; Mavromatis et al., 2015; Henehan et al., 2022), the $\delta^{11}B_{arag}$ allows for a direct reconstruction of the $\delta^{11}B_{brine}$. The $\delta^{11}B_{brine}$ was calculated from the $\delta^{11}B$ values of borate ion ($B(OH)_4^-$), the main species incorporated into inorganic aragonite ($\delta^{11}B_{borate} = \delta^{11}B_{arag}$), by solving the commonly used equation for calculating pH from $\delta^{11}B$ values:

$$pH = pK_B^* - \log\left[-\frac{\delta^{11}B_{brine} - \delta^{11}B_{borate}}{\delta^{11}B_{brine} - \left({}^{11-10}K_B \times \delta^{11}B_{borate}\right) - 10^3\left({}^{11-10}K_B - 1\right)}\right], \quad (1)$$

where pK_B^* is the dissociation constant for boric acid at an *in situ* temperature and salinity and ${}^{11-10}K_B$ is the isotopic fractionation factor (Klochko et al., 2006; Nir et al., 2015; here we use the value of 1.0272 ± 0.0006 from Klochko et al., 2006). The principles of boron isotope geochemistry and incorporation into $CaCO_3$ have been previously described in numerous publications (see e.g. Branson, 2018 and references therein); for further information the reader is directed to this literature.

The precipitation of aragonite from Dead Sea and Lake Lisan brines is known to occur under specific conditions only, after a substantial freshwater supply to the epilimnion during climatic conditions with increased precipitation or following wet winters in the region (Stein et al., 1997; Barkan et al., 2001). Inflowing freshwater through floods supplies the limiting HCO_3^- and temporarily reduces the ionic strength of the brine. While Dead Sea brines are characterised by an unusually low pH (around 6.5 at the surface and 6 at depth; Sass and Ben-Yaakov, 1977) and pK_B^* (~6.3; Golan et al., 2016), aragonite nucleation only occurs at specific conditions, with elevated pH and pK_B^* values. The conditions under which aragonite precipitation is favoured from Dead Sea and Lisan brines have been previously studied in detail (Ben Dor et al., 2021; Golan et al., 2016; Belmaker et al., 2019). Based on these studies, we consider that a dilution of the brines to 20% of Dead Sea brine (ionic strength, I = 1.72 mol kg^{-1}) and 40% of Lisan brine (I = 0.82 mol kg^{-1}) is required for a large-scale aragonite precipitation event to occur, corresponding to elevated brine pH of ~7.50. Taking these physical properties, and the corresponding ionic compositions of the diluted brines (from Ben Dor et al., 2021; Belmaker et al., 2019) the ensuing pK_B^* values were calculated using the PHREEQC program (Version 3; Parkhurst and Appelo, 2013) with the Pitzer database (pitzer.dat). The Dead Sea pK_B^* at 25 °C = 8.14, and Lisan pK_B^* at 25 °C = 8.53 and at 15 °C = 8.77 (Supp. Table 1). While most aragonite can be expected to precipitate as soon as favourable conditions with pH ~7.50 are achieved, some aragonite precipitation might potentially also take place at higher pH. A further dilution by half of the already diluted brines (i.e. a dilution of the original brines to remaining 10% of Dead Sea brine and 20% of Lisan brine) would give a pH of 7.75; the resulting $\delta^{11}B_{brine}$ is also shown for comparison.

2.3. Modelling

To quantitatively assess the relative roles of B cycle processes in setting $\delta^{11}B_{brine}$, we performed two separate isotope mass balance calculations of Lake Lisan, meant to inform its evolution following isolation in the Pliocene and the last high-stand of the late glacial period (see Supplement for further details).

In the first model (Pliocene, Model 1), the initial seawater volume enclosed in the Dead Sea basin at the point of isolation (Hall, 1996) is evaporated at a constant rate until it reaches its present-day volume, equivalent to a degree of evaporation (DE) of 14. The chemical evolution and precipitation of evaporites is set to follow the experimentally determined evaporative pathway, which indicates an onset of gypsum precipitation at a DE of 4, while halite begins to form at a DE of 9 (McCaffrey et al., 1987).

In the second model (late glacial, Model 2), we first infer the palaeohydrology of Lake Lisan over the last 25 ka from the lake level curve (Torfstein et al., 2013), which controls freshwater inflow, evaporation and sediment deposition. Next, the mass of aragonite, gypsum and halite forming during the same time period was inferred from the difference between amounts of Ca^{2+}, SO_4^{2-} and Na^+, respectively, present in the modern Dead Sea on one hand, and the combined amount of the same ions that was already present or added since the last glacial maximum on the other hand (Ben Dor et al., 2021). We assumed that evaporites formed mainly in time periods with a falling lake level, when evaporation exceeded freshwater discharge.

In each model we tracked the magnitude and isotopic composition of fluxes into and out of a single reservoir, representing Lake Lisan, and compared the resulting $\delta^{11}B_{brine}$ with the values reconstructed from lacustrine aragonites. Distribution and fractionation constants were either set or calculated using previously published values (Supplement).

3. Results and discussion

Using boron proxies ($\delta^{11}B$ to trace the isotope budget, and B/Ca and B/Li to infer changes in boron concentration) we follow the evolution of the brines from the last lake high-stand at the end of the Last Glacial Period to the late Holocene, reconstructed from aragonites deposited in the basin. Overall, we find broad variations in the B/Ca, B/Li and $\delta^{11}B_{arag}$, ranging between 330 and 3080 µmol/mol (Fig. 3a), 2 and 23 mol/mol (Fig. 3b), and 26.7‰ and 40.0‰ (n = 38; Fig. 3c), respectively, and with clearly distinct compositions between the two time intervals. The late glacial aragonites from Masada are characterised by statistically significantly lower $\delta^{11}B_{arag}$ (~31‰; p-value = $7.9 \times 10^{-7} < \alpha = 0.05$, t-Test) lower B/Ca (averaging ~400 µmol/mol p-value = $2.8 \times 10^{-4} < \alpha = 0.05$, t-Test) contrasting with the elevated B/Ca (~1300 µmol/mol) and $\delta^{11}B_{arag}$ (~36‰) of late Holocene aragonites from the ICDP Deep Core and Ein Gedi, and rather similar B/Li (~5–6 mol/mol; p-value = $0.49 > \alpha = 0.05$, t-Test). The measured $\delta^{11}B_{arag}$ are considerably heavier than marine carbonates (typically ranging between ~15–25‰; e.g. Hemming and Hanson, 1992; Branson, 2018), implying that they formed from solutions much higher in $\delta^{11}B$ than seawater. We note that some of the late Holocene aragonites, in particular those from the marginal site Ein Gedi show variable compositions; we refrain from interpreting these as more data is required to fully understand the cause of the observed variations and from here on, we focus on the main trend.

The reconstructed $\delta^{11}B_{brine}$ (from samples with Al/Ca <5,000 µmol/mol, see Supplement for further details, and based on the expected pH and pK_B^* conditions during aragonite precipitation during each time interval) result in mean composition of ~57‰ and ~60‰ for the late glacial Lake Lisan and late Holocene Dead Sea, respectively (Fig. 3d). These values are, as expected, well

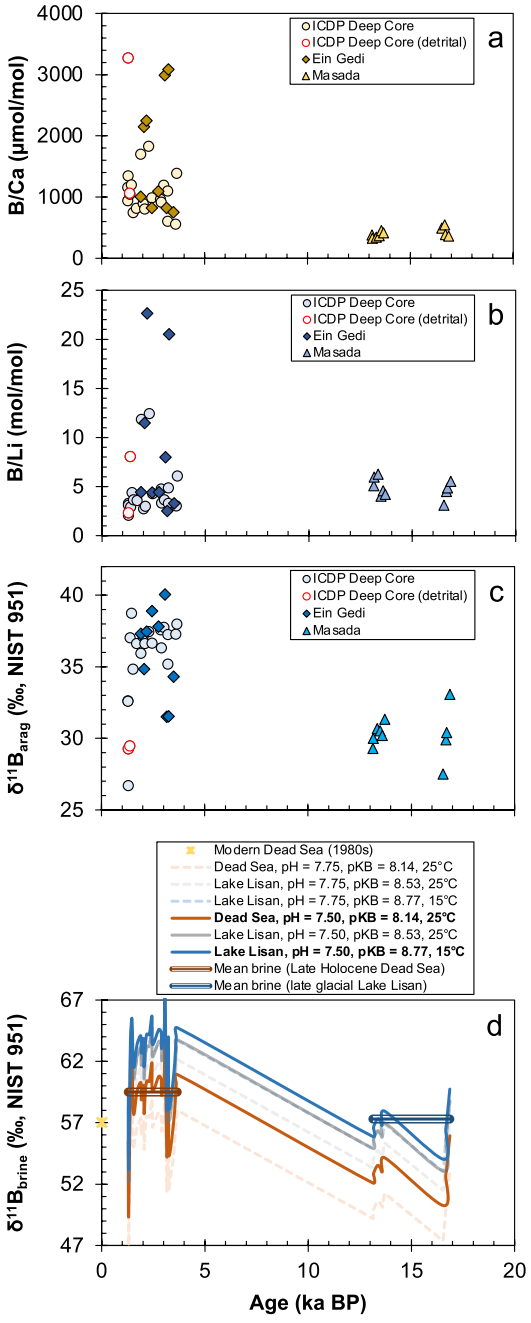

Fig. 3. Composition of aragonite laminae from the late Holocene Dead Sea and its late glacial precursor Lake Lisan; a) B/Ca; b) B/Li; c) measured $\delta^{11}B_{arag}$; d) reconstructed $\delta^{11}B_{brine}$ considering different pK_B^* and pH values (and temperatures for Lake Lisan), illustrating the effect of different pK_B^* and pH choice on the reconstructed $\delta^{11}B_{brine}$. The orange line between 1.5–3.5 ka BP gives the best estimate of Holocene $\delta^{11}B_{brine}$ (~57‰), and the dark blue line between ~13–17 ka BP of the late glacial Lake Lisan (~60‰) based on the scenarios highlighted in bold. For comparison, modern Dead Sea $\delta^{11}B_{brine}$ is ~57‰ and B/Li ~2–3 mol/mol (Vengosh et al., 1991b), while the ocean $\delta^{11}B_{sw}$ is much lower (39.6‰) and B/Li higher (17 mol/mol).

above the average seawater value (39.6‰), and close to slightly elevated than modern Dead Sea brines and the adjacent hot springs (55−58‰) reported by Vengosh et al. (1991b). Interestingly, the late Holocene brines show the highest values, while the late glacial $\delta^{11}B_{brine}$ appear more similar to the modern Dead Sea (57‰). These distinct $\delta^{11}B_{brine}$ values point to marked secular trends on millennial (the ~3‰ post-glacial increase) and million year time scales (the ~17‰ increase since its separation from seawater in Pliocene) and are accompanied by changes in the B budget of the brine.

From measurements of recent brines it is apparent that since their evolution from seawater, the brines became not only isotopically enriched, but also about an order of magnitude more concentrated in B than the ocean (~41.1 ppm vs. 4.5 ppm, respectively; Vengosh et al., 1991b). Although changes in the boron concentration of the brines $[B]_{brine}$ are not straightforward to reconstruct, the post-glacial increase in aragonite B/Ca could possibly hint at further increase in $[B]_{brine}$ during the Holocene, when the brines also became more concentrated in other major conservative ions (Levy et al., 2017). Previously, changes in B/Ca of synthetic aragonites have been found to principally dependent on the relative concentration of $[B(OH)_4^-]$ and $[CO_3^{2-}]$ and hence result from changes in carbonate chemistry (Holcomb et al., 2016). However, if aragonite precipitation only occurs under specific carbonate system conditions (as in the Dead Sea), increase in total $[B]_{brine}$ – and by default more $[B(OH)_4^-]$ (at a given pH/set of carbonate system conditions) – could potentially lead to more $[B(OH)_4^-]$ being incorporated into aragonites, resulting in higher B/Ca values. The rather similar B/Li values of aragonites also support conservative behaviour of B during this time interval.

To unravel the underlaying processes responsible for the evolution of B in the Dead Sea basin we set up two separate simple mass balance calculations modelling the long-term boron cycle since the lagoon formation in the Pliocene (Model 1; Fig. 4a and 4b), and since the last lake high-stand following the LGM (Model 2; Fig. 4c and 4d). In each model, we take into account the hydrological changes in the basin at the time and the main known B fluxes; coprecipitation of B in evaporitic minerals '*Evaporites*', B loss in vapour '*Vapor loss*', adsorption of B on clay sediments '*Sediments*' and freshwater B input '*Inflow*' (Supplement). We then model $\delta^{11}B_{brine}$ and $[B]_{brine}$ trajectories by selectively adding or removing the different B fluxes to study their individual and combined impact on the B budget.

Our results show that the evolution of Dead Sea brines is best explained by the combination of all known B input and output fluxes. The main process responsible for the unique B composition of modern Dead Sea brines accounting for more than 50% of the post-Pliocene $\delta^{11}B_{brine}$ enrichment is B adsorption onto clay minerals, a well-known sink for ^{10}B which leaves solutions enriched in ^{11}B (Palmer et al., 1987). To a lesser degree, ^{10}B loss to atmospheric water vapour which is depleted in ^{11}B relative to the liquid (Rose-Koga et al., 2006), and coprecipitation of ^{10}B in evaporitic deposits also act as sinks for light B, contributing to the brine enrichment. Carbonates are well-known to incorporate the relatively lighter tetrahedral $B(OH)_4^-$ which is more compatible in the crystal lattice than the trigonal $B(OH)_3$, and gypsum can be expected to behave similarly. In halite, B is expected to be predominantly incorporated in fluid inclusions rather than the crystal lattice, and hence involve both $B(OH)_4^-$ and $B(OH)_3$ without significant fractionation from brine, with negligible impact on the $\delta^{11}B_{brine}$ budget (Paris et al., 2010). Thus, the evaporite ^{10}B sink mainly consists of carbonate and gypsum phases and is not expected to be affected by halite precipitation.

The reconstructed $\delta^{11}B_{brine}$ enrichment (of about ~3‰) from the end of the last glaciation to the late Holocene can be principally explained by a reduction in riverine discharge into the basin. The lower Jordan River contains considerable amounts of B (~2 ppm) and has light $\delta^{11}B$ values (~35‰) relative to the brines (Farber et al., 2004) – these values are relatively high in comparison to other rivers globally (Lemarchand et al., 2000) – likely due to draining over substantial areas of the exposed Lisan Formation. To support the Lake Lisan high-stand, glacial inflow must have been considerably higher than during the Holocene and thus the Lisan $\delta^{11}B_{brine}$ lower. Post-glacial decrease in Jordan River in-

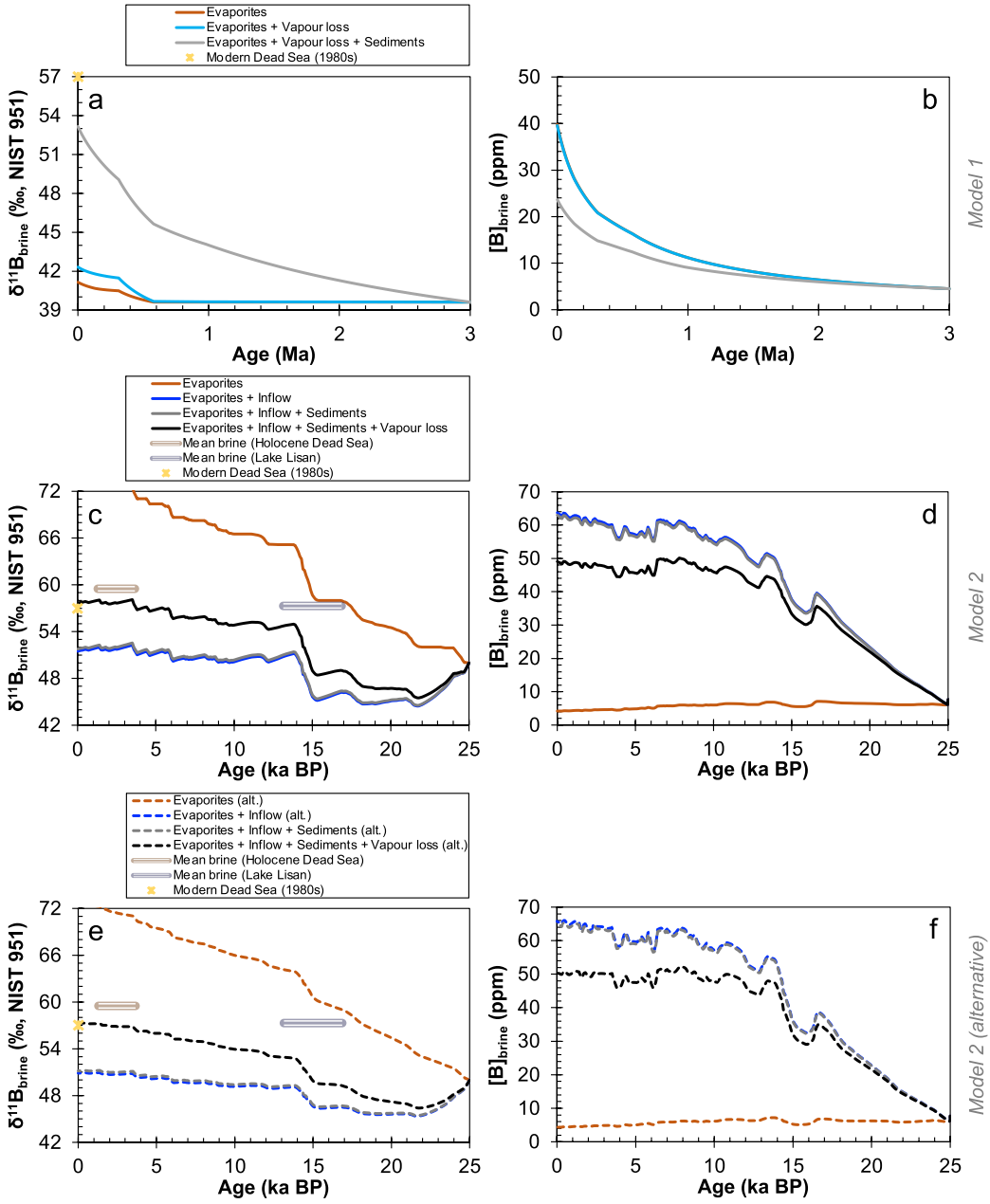

Fig. 4. Secular evolution of boron in the Dead Sea basin. Model 1: a) modelled $\delta^{11}B_{brine}$ and b) $[B]_{brine}$ over the last 3 Myr. Model 2: c) modelled $\delta^{11}B_{brine}$ and d) $[B]_{brine}$ over the last 25 ka BP. The impact of the main boron fluxes and their combination on the lake boron budget is shown by the different lines. In both models, the combination of all known boron fluxes (grey line in Model 1 and black line in Model 2) produces trajectories most consistent with observations. Model 2 alternative: an alternative run of Model 2 showing e) $\delta^{11}B_{brine}$ and f) $[B]_{brine}$ evolution over the last 25 ka BP. Unlike the previous (Model 2) run where aragonite is treated as a purely evaporitic deposit, here aragonite formation is scaled to freshwater input to account for aragonite formation during glacial times. 1-sigma uncertainty envelopes are <1‰ (16, 50 and 84% distributions are available in the Supplement).

flow together with an increase in the ^{10}B sink from '*Evaporites*' and '*Vapour loss*' driven by transition from cooler and wetter to warmer and drier climate in the Levant leads to the enriched late Holocene $\delta^{11}B_{brine}$. The approximately half (~200 m), reduction in the lake level height and hence lake volume across the transition also leads to a conservative increase in $[B]_{brine}$, which maintains the importance of the output fluxes despite the decline in the input flux.

In this model, aragonite formation is treated as an evaporitic deposit (Ben Dor et al., 2021) and thus its formation is linked to warming, evaporation and dropping lake level. Dissolved inorganic carbon (DIC) supply is however thought to exert the main control on aragonite formation during glacial times. To test for this effect, we carried out an alternative model run (Model 2 alternative) where the aragonite formation is scaled to freshwater input. The impact of this effect on the lake boron budget is minimal and the results broadly agree with those obtained from the previous run (Fig. 4e and 4f).

We note that although the combination of all fluxes in Model 2 ('*Evaporites*' + '*Inflow*' + '*Sediments*' + '*Vapour loss*'; Fig. 4c and 4d) largely tracks the reconstructed $\delta^{11}B_{brine}$, it does not exactly match the reconstructed values. This is not unexpected considering the limited constraints we have at present on B cycling in the Dead Sea (and in nature more generally). For the same reasons, it is currently difficult to fully assess the model uncertainties. Better knowledge of B fluxes as well as the lake palaeohydrology is needed before the model can be refined. Nevertheless, our mass balance calculation clearly illustrates the effect of known B fluxes on the Dead Sea B budget, both individually and when combined

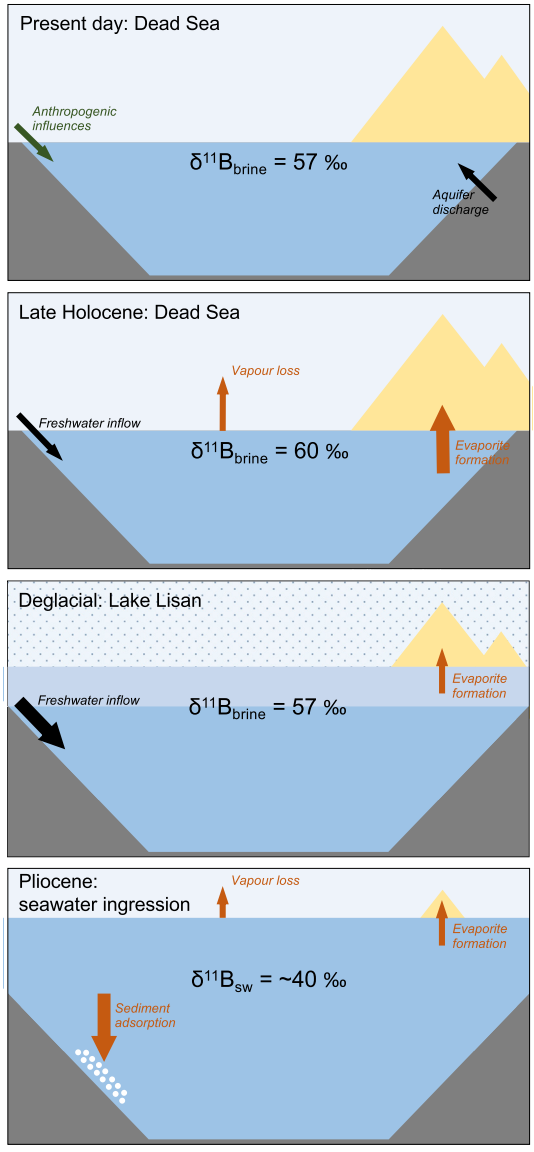

Fig. 5. Geological evolution of the Dead Sea boron budget. The relative importance of the different processes (as assessed here) is indicated by the arrow size. Orange arrows indicate main (light) boron sinks. Black arrows indicate water inflow processes that supply boron to the lake; dark green arrow indicates possible additional modern boron input from anthropogenic activities.

(Fig. 5), and that it is the latter that best explains the evolution of the brines.

Why modern $\delta^{11}B_{brine}$ (~57‰; Vengosh et al., 1991b) is lower than the late Holocene despite increasing evaporitic influence in the region (and its consequent impact on the main B fluxes) is challenging to explain without further knowledge of historic $\delta^{11}B_{brine}$. Considering that Vengosh et al. (1991b) measured the brines in the 1980s, it is possible that their chemistry no longer reflects a natural evaporitic evolution and that the impact of anthropogenic activities (e.g., potash mining) and water usage on the B budget needs to be taken into account. For instance, Farber et al. (2004) hypothesized that gypsum-rich marly sediments with a light $\delta^{11}B$ (~30‰) could be dissolving due to seepage of agricultural wastewaters into the ground, which would lead to contribution of relatively light B to the lake. Drawing lessons from the late glacial Lake Lisan, a drop in $\delta^{11}B_{brine}$ would be expected with an increased inflow into the lake. One of the main indirect consequences of the increased recent anthropogenic water usage is the lake level fall, and as a result increased flow of recycled glacial groundwater through springs (e.g. the Ein-Qedem spring) into the lake (Weber et al., 2018). These springs are relatively light in $\delta^{11}B_{brine}$ (~52‰) and high in [B] (~20 ppm; Vengosh et al., 1991b) with respect to the lake brine and their increased seepage into the lake could convincingly explain the recent decline in $\delta^{11}B_{brine}$ values.

4. Conclusions

We investigated the $\delta^{11}B$ (along with Element/Ca, $\delta^{13}C$ and $\delta^{18}O$; see Supplement) composition of authigenic aragonites deposited within the Dead Sea basin during the late glacial Lake Lisan high-stand and the late Holocene Dead Sea low-stand. We show that Dead Sea sedimentary sequences contain structurally and chemically pristine aragonites suitable for geochemical analyses which, given their tight controls on precipitation, allow for the reconstruction of past $\delta^{11}B_{brine}$. We find considerable variations in the lake boron budget on million and millennial year time scales driven by changing relative importance of the main boron fluxes. Modelling shows that external input of solids and solutes is required to produce brines strongly enriched in $\delta^{11}B$. The marked departure of the modern $\delta^{11}B_{brine}$ from the initial $\delta^{11}B_{seawater}$ during the evolution of the lake can be largely explained by sustained clay mineral discharge into the basin (at current rate). To quantitatively disentangle the various boron mass fluxes and their contributions to the brine composition, constraints on the lake palaeohydrology during the last 3 million years, such as intermittent reconnection to the Mediterranean are required, which are at present lacking. Millennial trends in $\delta^{11}B_{brine}$ can be largely attributed to changes to the riverine inflow and as a result the lake volume, driven by broad hydro-climatic shifts in the Eastern Mediterranean. Our study contributes to the understanding of boron cycling in nature, highlights the value of boron geochemistry in lacustrine systems as a tracer of key basin processes and the important role of sediments on geological time scales, which also deserve further attention when constraining the marine boron budget.

CRediT authorship contribution statement

Hana Jurikova: Writing – review & editing, Writing – original draft, Methodology, Formal analysis, Conceptualization. **Simon J. Ring:** Writing – review & editing, Methodology, Formal analysis. **Michael J. Henehan:** Writing – review & editing, Methodology. **Ina Neugebauer:** Writing – review & editing, Methodology. **Birgit Schröder:** Writing – review & editing, Methodology. **Daniela Müller:** Writing – review & editing, Methodology. **Markus J. Schwab:** Writing – review & editing, Resources. **Rik Tjallingii:** Writing – review & editing, Resources. **Achim Brauer:** Writing – review & editing, Resources. **Cécile Blanchet:** Writing – review & editing, Resources.

Declaration of competing interest

The authors declare that they have no known competing financial interests or personal relationships that could have appeared to influence the work reported in this paper.

Data availability

Data generated in this study as well as further information on aragonite samples and modelling is available in the Supplementary material (Appendix A.).

Acknowledgements

We thank Brian Brandemann, Sylvia Pinkerneil (GFZ Potsdam, Section 4.3), Ilona Schäpan (GFZ Potsdam, Section 3.5), and Jutta

Schlegel and Daniel Frick (GFZ Potsdam, Section 3.3) for support on field and/or laboratory work. This project was funded by the German Research Foundation, DFG (Grant no. TJ 66/2-1, 'Sediment provenance and past hydrological balance in the Dead Sea region during the Early Holocene' - PRO-HYDRO) under Priority Programme 1006 ICDP, and was also supported by the DFG project PALEX (Grant no. BR2208/13-1/-2, 'Paleohydrology and Extreme Floods from the Dead Sea ICDP core').

Appendix A. Supplementary material

Supplementary material related to this article can be found online at https://doi.org/10.1016/j.epsl.2023.118403.

References

Barkan, E., Luz, B., Lazar, B., 2001. Dynamics of the carbon dioxide system in the Dead Sea. Geochim. Cosmochim. Acta 65, 355–368. https://doi.org/10.1016/S0016-7037(00)00540-8.

Belmaker, R., Lazar, B., Stein, M., Taha, N., Bookman, R., 2019. Constraints on aragonite precipitation in the Dead Sea from geochemical measurement of flood plumes. Quat. Sci. Rev. 221, 105876. https://doi.org/10.1016/j.quascirev.2019.105876.

Ben Dor, Y., Neugebauer, I., Enzel, Y., Schwab, M.J., Tjallingii, R., Erel, Y., Brauer, A., 2019. Varves of the Dead Sea sedimentary record. Quat. Sci. Rev. 215, 173–184. https://doi.org/10.1016/j.quascirev.2019.04.011.

Ben Dor, Y., Flax, T., Levitan, I., Enzel, Y., Brauer, A., Erel, Y., 2021. The paleohydrological implications of aragonite precipitation under contrasting climates in the endorheic Dead Sea and its precursors revealed by experimental investigations. Chem. Geol. 576, 120261. https://doi.org/10.1016/j.chemgeo.2021.120261.

Branson, O., 2018. Boron Incorporation into Marine $CaCO_3$. In: Marschall, H., Foster, G. (Eds.), Boron Isotopes. Advances in Isotope Geochemistry. Springer, Cham, pp. 71–105.

Buisson, M., Louvat, P., Thaler, C., Rollion-Bard, C., 2021. High precision MC-ICP-MS measurements of $^{11}B/^{10}B$ ratios from ng amounts of boron in carbonate samples using microsublimation and direct injection (μ-dDIHEN). J. Anal. At. Spectrom. https://doi.org/10.1039/D1JA00109D.

Farber, E., Vengosh, A., Gavrieli, I., Marie, A., Bullen, T.D., Mayer, B., Holtzman, R., Segal, M., Shavit, U., 2004. The origin and mechanism of salinization of the lower Jordan River. Geochim. Cosmochim. Acta 68, 1989–2006. https://doi.org/10.1016/j.gca.2003.09.021.

Foster, G.L., Pogge von Strandmann, P.A.E., Rae, J.W.B., 2010. Boron and magnesium isotopic composition of seawater. Geochem. Geophys. 11, Q08015. https://doi.org/10.1029/2010GC003201.

Golan, R., Gavrieli, I., Ganor, J., Lazar, B., 2016. Controls on the pH of hyper-saline lakes – a lesson from the Dead Sea. Earth Planet. Sci. Lett. 434, 289–297. https://doi.org/10.1016/j.epsl.2015.11.022.

Gutjahr, M., et al., 2020. Sub-permil interlaboratory consistency for solution-based boron isotope analyses on marine carbonates. Geostand. Geoanal. Res. 45, 59–75. https://doi.org/10.1111/ggr.12364.

Hall, J.K., 1996. Digital topography and bathymetry of the area of the Dead Sea Depression. Tectonophysics 266, 177–185. https://doi.org/10.1016/S0040-1951(96)00189-8.

Hemming, N.G., Hanson, G.N., 1992. Boron isotopic composition and concentration in modern marine carbonates. Geochim. Cosmochim. Acta 56, 537–543. https://doi.org/10.1016/0016-7037(92)90151-8.

Henehan, M.J., Klein Gebbinck, C.D., Wyman, J.V.B., Hain, M.P., Rae, J.W.B., Hönisch, B., Foster, G., Kim, S.-T., 2022. No ion is an island: multiple ions influence boron incorporation into $CaCO_3$. Geochim. Cosmochim. Acta 318, 510–530. https://doi.org/10.1016/j.gca.2021.12.011.

Holcomb, M., DeCarlo, T.M., Gaetani, G.A., McCulloch, M., 2016. Factors affecting B/Ca rations in synthetic aragonite. Chem. Geol. 437, 67–76. https://doi.org/10.1016/j.chemgeo.2016.05.007.

Jurikova, H., Liebetrau, V., Gutjahr, M., Rollion-Bard, C., Hu, M.Y., Krause, S., Henkel, D., Hiebenthal, C., Schmidt, M., Laudien, J., Eisenhauer, A., 2019. Boron isotope systematics of cultured brachiopods: response to acidification, vital effects and implications for palaeo-pH reconstruction. Geochim. Cosmochim. Acta 248, 370–386. https://doi.org/10.1016/j.gca.2019.01.015.

Katz, A., Starinsky, A., 2009. Geochemical history of the Dead Sea. Aquat. Geochem. 15, 159–194. https://doi.org/10.1007/s10498-008-9045-0.

Kaufman, A., 1971. U-series dating of Dead Sea basin carbonates. Geochim. Cosmochim. Acta 35, 1269–1281. https://doi.org/10.1016/0016-7037(71)90115-3.

Kiro, Y., Goldstein, S.L., Garcia-Veigas, J., Levy, E., Kushnir, Y., Stein, M., Lazar, B., 2017. Relationships between lake-level changes and water and salt budgets in the Dead Sea during extreme aridities in the Eastern Mediterranean. Earth Planet. Sci. Lett. 464, 211–226. https://doi.org/10.1016/j.epsl.2017.01.043.

Kitagawa, H., Stein, M., Goldstein, S.L., Nakamura, T., Lazar, B., DSDDP Scientific Party, 2017. Radiocarbon chronology of the DSDDP core at the deepest floor of the Dead Sea. Radiocarbon 59, 383–394. https://doi.org/10.1017/RDC.2016.120.

Klochko, K., Kaufman, A.J., Wengsheng, Y., Byrne, R.H., Tossell, J.A., 2006. Experimental measurement of boron isotope fractionation in seawater. Earth Planet. Sci. Lett. 248, 276–285. https://doi.org/10.1016/j.epsl.2006.05.034.

Lemarchand, D., Gaillardet, J., Lewin, É., Allègre, C.J., 2000. The influence of rivers on marine boron isotopes and implications for reconstructing past ocean pH. Nature 408, 951–954. https://doi.org/10.1038/35050058.

Leslie, D., Lyons, W.B., Warner, N., Vengosh, A., Olesik, J., Welch, K., Deuerling, K., 2014. Boron isotopic geochemistry of the McMurdo Dry Lake Valleys, Antarctica. Chem. Geol. 386, 152–164. https://doi.org/10.1016/j.chemgeo.2014.08.016.

Levy, E.J., Stein, M., Lazar, B., Gavrieli, I., Yechieli, Y., Sivan, O., 2017. Pore fluids in Dead Sea sediment core reveal linear response of lake chemistry to global climate changes. Geology 45, 315–318. https://doi.org/10.1130/G38685.1.

Levy, E.J., Sivan, O., Antler, G., Lazar, B., Stein, M., Yechieli, Y., Gavrieli, I., 2019. Mount Sedom salt diapir-Source for sulfate replenishment and gypsum supersaturation in the last glacial Dead Sea (Lake Lisan). Quat. Sci. Rev. 221, 105871. https://doi.org/10.1016/j.quascirev.2019.105871.

Mavromatis, V., Montouillout, V., Noreaux, J., Gaillardet, J., Schott, J., 2015. Characterization of boron incorporation and speciation in calcite and aragonite from co-precipitation experiments under controlled pH, temperature, and precipitation rate. Geochim. Cosmochim. Acta 150, 299–313. https://doi.org/10.1016/j.gca.2014.10.024.

McCaffrey, M.A., Lazar, B., Holland, H.D., 1987. The evaporation path of seawater and the coprecipitation of Br^- and K^+ with halite. J. Sediment. Petrol. 57, 928–937. https://doi.org/10.1306/212F8CAB-2B24-11D7-8648000102C1865D.

Migowski, C., Stein, M., Prasad, S., Negendank, J.F.W., Agnon, A., 2006. Holocene climate variability and cultural evolution in the near East from the Dead Sea sedimentary record. Quat. Res. 66, 421–431. https://doi.org/10.1016/j.yqres.2006.06.010.

Misra, S., Owen, R., Kerr, J., Greaves, M., Elderfield, H., 2014. Determination of $\delta^{11}B$ by HR-ICP-MS from mass limited samples: application to natural carbonates and water samples. Geochim. Cosmochim. Acta 140, 531–552. https://doi.org/10.1016/j.gca.2014.05.047.

Müller, D., Neugebauer, I., Ben Dor, Y., Enzel, Y., Schwab, M.J., Tjallingii, R., Brauer, A., 2022. Phases of stability during major hydroclimate change ending the Last Glacial in the Levant. Sci. Rep. 12, 6052. https://doi.org/10.1038/s41598-022-10217-9.

Neev, D., Emery, K.O., 1967. The Dead Sea, depositional processes and environments of evaporites. Geol. Surv. Isr. Bull. 41, 1–147.

Neugebauer, I., et al., 2014. Lithology of the long sediment record recovered by the ICDP Dead Sea Deep Drilling Project (DSDDP). Quat. Sci. Rev. 102, 149–165. https://doi.org/10.1016/j.quascirev.2014.08.013.

Neugebauer, I., et al., 2015. Evidence for centennial dry periods at ~3300 and ~2800 cal. yr BP from micro-facies analyses of the Dead Sea Sediments. Holocene 25, 1358–1371. https://doi.org/10.1177/0959683615584208.

Neugebauer, I., Müller, D., Schwab, M.J., Blockley, S., Lane, C.S., Wulf, S., Appelt, O., Brauer, A., 2021. Cryptotephras in the Late glacial ICDP Dead Sea sediment record and their implications for chronology. Boreas 50, 844–861. https://doi.org/10.1111/bor.12516.

Nir, O., Vengosh, A., Harkness, J.S., Dwyer, G.S., Lahav, O., 2015. Direct measurement of the boron isotope fractionation factor: reducing the uncertainty in reconstructing ocean paleo-pH. Earth Planet. Sci. Lett. 414, 1–5. https://doi.org/10.1016/j.epsl.2015.01.006.

Noireaux, J., Mavromatis, V., Gaillardet, J., Schott, J., Montouillout, V., Louvat, P., Rollion-Bard, C., Neuville, D.R., 2015. Crystallographic controls on the boron isotope paleo-pH proxy. Earth Planet. Sci. Lett. 430, 398–407. https://doi.org/10.1016/j.epsl.2015.07.063.

Palmer, M.R., Spivack, A.J., Edmond, J.M., 1987. Temperature and pH controls over isotopic fractionation during adsorption on marine clay. Geochim. Cosmochim. Acta 51, 2319–2323. https://doi.org/10.1016/0016-7037(87)90285-7.

Paris, G., Gaillardet, J., Louvat, P., 2010. Geological evolution of seawater boron isotopic composition recorded in evaporate. Geology 38. https://doi.org/10.1130/G31321.1.

Parkhurst, D.L., Appelo, C.A.J., 2013. Description of Input and Examples for PHREEQC Version 3: a computer program for speciation, batch-reaction, one-dimensional transport, and inverse geochemical calculations. In: U.S. Geological Survey Techniques and Methods, Book 6, Chapter A43. 497 p. https://pubs.usgs.gov/tm/06/a43/.

Ramsey, C.B., 2008. Radiocarbon dating: revolutions in understanding. Archaeometry 50, 249–275. https://doi.org/10.1111/j.1475-4754.2008.00394.x.

Rose-Koga, E.F., Sheppard, S.M.F., Chaussidon, M., Carignan, J., 2006. Boron isotopic composition of atmospheric precipitations and liquid-vapor fractionations. Geochim. Cosmochim. Acta 70, 1603–1615. https://doi.org/10.1016/j.gca.2006.01.003.

Sass, E., Ben-Yaakov, S., 1977. The carbonate system in hypersaline solutions: Dead Sea brines. Mar. Chem. 5, 183–199. https://doi.org/10.1016/0304-4203(77)90006-8.

Stein, M., Starinsky, A., Katz, A., Goldstein, S.L., Machlus, M., Schramm, A., 1997. Sr-isotopic, chemical, and sedimentological evidence for the evolution of Lake Lisan

and the Dead Sea. Geochim. Cosmochim. Acta 61, 3975–3992. https://doi.org/10.1016/S0016-7037(97)00191-9.

Swihart, G.H., Moore, P.B., Callis, E.L., 1986. Boron isotopic composition of marine and non-marine evaporite borates. Geochim. Cosmochim. Acta 50, 1297–1301. https://doi.org/10.1016/0016-7037(86)90413-8.

Torfstein, A., Gavrieli, I., Katz, A., Kolodny, Y., Stein, M., 2008. Gypsum as a monitor of paleo-limnological-hydrological conditions in Lake Lisan and the Dead Sea. Geochim. Cosmochim. Acta 72, 2491–2509. https://doi.org/10.1016/j.gca.2008.02.015.

Torfstein, A., Goldstein, S.L., Stein, M., Enzel, Y., 2013. Impacts of abrupt climate changes in the Levant from Last Glacial Dead Sea levels. Quat. Sci. Rev. 69, 1–7. https://doi.org/10.1016/j.quascirev.2013.02.015.

Trumbull, R.B., Slack, J.F., 2017. Boron isotopes in the continental crust: granites, pegmatites, felsic volcanic rocks, and related ore deposits. In: Marschall, H., Foster, G. (Eds.), Boron Isotopes. Advances in Isotope Geochemistry. Springer, Cham, pp. 249–272.

Vengosh, A., Chivas, A.R., McCulloch, M.T., Starinsky, A., Kolodny, Y., 1991a. Boron isotope geochemistry of Australian salt lakes. Geochim. Cosmochim. Acta 55, 2591–2606. https://doi.org/10.1016/0016-7037(91)90375-F.

Vengosh, A., Starinsky, A., Kolodny, Y., Chivas, A.R., 1991b. Boron isotope geochemistry as a tracer for the evolution of brines and associated hot springs from the Dead Sea, Israel. Geochim. Cosmochim. Acta 55, 1689–1695. https://doi.org/10.1016/0016-7037(91)90139-V.

Vengosh, A., Starinsky, A., Kolodny, Y., Chivas, A.R., Raab, M., 1992. Boron isotope variations during fractional evaporation of sea water: new constrains on the marine vs. nonmarine debate. Geology 20, 799–802. https://doi.org/10.1130/0091-7613(1992)020<0799:BIVDFE>2.3.CO;2.

Vengosh, A., Chivas, A.R., Starinsky, A., Kolodny, Y., Baozhen, Z., Zhang, Pengxi, 1995. Chemical and boron isotope composition of non-marine brines from the Qaidam Basin, Qinghai, China. Chem. Geol. 120, 135–154. https://doi.org/10.1016/0009-2541(94)00118-R.

Wang, B.-S., et al., 2010. Direct separation of boron from Na- and Ca-rich matrices by sublimation for stable isotope measurement by MC-ICP-MS. Talanta, 1378–1384. https://doi.org/10.1016/j.talanta.2010.07.010.

Weber, N., Yechieli, Y., Stein, M., Yokochi, R., Gavrieli, I., Zappala, J., Mueller, P., Lazar, B., 2018. The circulation of the Dead Sea brine in the regional aquifer. Earth Planet. Sci. Lett. 493, 242–261. https://doi.org/10.1016/j.epsl.2018.04.027.

Zak, I., 1967. The Geology of Mount Sedom. Unpublished Ph.D. thesis. Hebrew University of Jerusalem.

Zeebe, R.E., Rae, J.W.B., 2020. Equilibria, kinetics, and boron isotope partitioning in the aqueous boric acid-hydrofluoric acid system. Chem. Geol. 550, 119693. https://doi.org/10.1016/j.chemgeo.2020.119693.